Active Lighting Applied to 3D Reconstruction of Specular Metallic Surfaces by Polarization Imaging

Olivier Morel, Christophe Stolz, Fabrice Meriaudeau, Patrick Gorria

Le2i UMR CNRS 5158, 12 rue de la Fonderie,
71200 Le Creusot, France

o.morel@iutlecreusot.u-bourgogne.fr

In the field of industrial vision, the three-dimensional inspection of highly reflective metallic objects is still a delicate task. This paper deals with a new automated 3D inspection system based on polarization analysis. We first present an extension of the 'Shape from Polarization' method for dielectric to metallic surfaces. Then, we describe a new way of solving the ambiguity concerning the normals orientation, with an active lighting system. Finally, applications on shape defects detection are discussed, and the efficiency of the system to discriminate defects on specular metallic objects made by stamping and polishing is presented.

OCIS codes: 110.6880

1. Introduction

The 3D machine vision systems market is expanding rapidly, providing 3D-based machine vision for process control. Nevertheless, the inspection of specular metallic objects remains a delicate task, since it requires to control the whole lighting of the scene. Extracting the shape information of specular metallic surfaces from a single view is still a challenging problem, and there are currently two kinds of techniques. The first one is to study the highlights of structured lightings, with multiple ring lights,[1] with a hemisphere of 127 point sources like the SHINY system,[2] or with a calibrated pattern composed of lines.[3,4] The second technique is to study the motion of a specularly reflected pattern on the surface which is different of the real motion of the object.[5] Here, we propose a new way of reconstructing the 3D information on specular metallic objects, by extending the 'Shape from Polarization' method to metallic surfaces. Koshikawa[6] first used polarization information to determine the shape of dielectric glossy objects. Shape information were computed by analyzing the stokes parameters of a circularly polarized light reflected by the object surface. Later, Wolff[7] has shown how

the surface normals are constraint to the polarimetric parameters of an unpolarized light reflected by the surface. This 'Shape from Polarization' method was especially developed by Miyazaki,[8,9] and Rahmann[10,11] for transparent or reflective surfaces, but of dielectric nature. By using the complex refractive index of the surface, we have found new relations between the polarization images and the surface normals.[12,13,14] The previous authors don't provide any robust solution to solve the ambiguity concerning the determination of the normal azimuth angle. We propose here, a new way of solving it by using an active lighting system. Once the surface normals are computed, the surface is reconstructed by integration.

The paper is organized as follows: the 'Shape from Polarization' method extended to specular metallic surfaces is presented in section 2. Section 3 describes the active lighting system to solve the ambiguity of the azimuth angle. The description of the whole acquisition system, and the results are exposed in section 4.

2. 'Shape from Polarization' for metallic surfaces

The surface is assumed to be continuous, and is described by a cartesian expression: $z = f(x, y)$. Therefore, each surface normal (Fig. 1) is given by the following non-normalized expression:

$$\overrightarrow{n} = \begin{pmatrix} -\frac{\partial f(x,y)}{\partial x} \\ -\frac{\partial f(x,y)}{\partial y} \\ 1 \end{pmatrix} = \begin{pmatrix} p = tan\theta_r cos\phi \\ q = tan\theta_r sin\phi \\ 1 \end{pmatrix}. \quad (1)$$

This expression establishes the relationship between the normal orientation (given by the zenith angle θ_r and the azimuth angle ϕ), and the partial derivatives of the surface. This section presents the two main steps of the 'Shape from Polarization' method. Firstly, we demonstrate how to compute the surface normals (especially for the metallic one), thanks to the polarization properties of the reflected light. Secondly, we describe an algorithm in order to reconstruct the 3D shape by integrating the normals.

2.A. Polarization Imaging

After being reflected, an unpolarized light wave becomes partially linearly polarized, depending on the surface normal and on the refractive index of the media it impinges on. A partially linearly polarized light wave has three parameters:

- the light magnitude I,
- the degree of polarization ρ,
- and the angle of polarization φ.

The degree of polarization varies from 0 for a completely unpolarized light, to 1 for a perfectly linearly polarized light. To study the polarization state of such a wave, the use of a rotating polarizer in front of a camera is enough.[15] The relationship between the magnitude I_p of the transmission of a partially linearly polarized light wave through a rotating polarizer, and the angle α of the polarizing filter is given by a sinusoid (Fig. 2):

$$I_p(\alpha) = \frac{I_{max} - I_{min}}{2} \cos(2\alpha - 2\varphi) + \frac{I_{max} + I_{min}}{2}, \tag{2}$$

where I_{min} and I_{max} represent, respectively, the minimum and the maximum magnitude seen through the polarizer. Equation (2) can be written in the form:

$$I_p(\alpha) = \frac{I}{2} \left(\rho \cos(2\alpha - 2\varphi) + 1\right), \tag{3}$$

with:

$$I = I_{max} + I_{min}, \qquad \rho = \frac{I_{max} - I_{min}}{I_{max} + I_{min}}. \tag{4}$$

The purpose of polarization imaging is to compute the three parameters: I, φ, and ρ, by interpolating the formula (3). There are several methods to fit the equation in order to get the parameters. Because, there are three parameters, at least three images, taken with different orientations of the polarizer, are required. Since the degree of polarization is low for metallic surfaces, and to improve the accuracy of the measure of the parameters, we apply the linear least squares method, by taking 18 frames with a constant step of 10 degrees.

2.A.1. Relationship between the angle of polarization φ and the azimuth angle ϕ

Wolff[7] has demonstrated how to determine constraints on surface normals by using the Fresnel reflectance model. The Fresnel coefficients of reflection $F_\perp$and $F_\parallel$, are the ratio between the amplitude of the reflected light and the incident light, according respectively to the perpendicular and the parallel plane to the plane of incidence:

$$\left.\begin{aligned} F_\perp &= \left|\frac{\sin(\theta_i - \theta_t)}{\sin(\theta_i + \theta_t)}\right|^2, \\ F_\parallel &= \left|\frac{\tan(\theta_i - \theta_t)}{\tan(\theta_i + \theta_t)}\right|^2. \end{aligned}\right\} \tag{5}$$

where θ_i is the angle of incidence, and θ_t is the angle of refraction. The Fresnel formulae 5 show that the orthogonal component $F_\perp$ is greater than the parallel one $F_\parallel$. Therefore, it means that an unpolarized light wave becomes partially linearly polarized according to the normal of the plane of incidence. Thus, the azimuth angle ϕ can be inferred from the angle of polarization φ:

$$\phi = \varphi \pm \frac{\pi}{2}. \tag{6}$$

A new technique to disambiguate this relation will be presented in the next section.

2.A.2. Relationship between the degree of polarization ρ and the zenith angle θ_r

The disparity between the components $F_\perp$ and $F_\parallel$ brings also a new piece of information: the degree of polarization of the reflected light. Indeed, the degree of polarization can be expressed as follows:

$$\rho = \frac{F_\perp - F_\parallel}{F_\perp + F_\parallel}. \tag{7}$$

To find a new relationship between the degree of polarization and the zenith angle for metallic surfaces, we introduce the complex refractive index: $\hat{n} = n(1 + i\kappa)$ (where κ is called the attenuation index). By assuming the refractive index of the air to be 1, we can write the Snell-Descartes's law :

$$\sin\theta_i = \hat{n}\sin\theta_t, \tag{8}$$

where θ_i and θ_t are respectively the incident and refractive angles. In order to simplify the relations, and as it is usually the case in the visible region, the following approximation[16] is applied:

$$|\hat{n}|^2 = n^2(1 + \kappa^2) \gg 1. \tag{9}$$

Thanks to this approximation, by substituting equation (5) into equation (7), and by writing $\theta_i = \theta_r$ with the Snell-Descartes's law (8), the degree of polarization ρ for metallic surfaces can be expressed as follows:

$$\rho(\theta_r) = \frac{2n\tan\theta_r\sin\theta_r}{\tan^2\theta_r\sin^2\theta_r + |\hat{n}|^2}. \tag{10}$$

Fig. 3 shows that the difference between the true degree of polarization and its approximation grows slightly only for great values of the angle θ_r. The curve also shows that the ambiguity concerning the determination of the angle θ_r, according to the degree of polarization ρ, doesn't have to be treated for surfaces with slopes lower than 80°, as it is the case with the studied objects. For most of metallic surfaces, the peak appears generally at higher angle than for the dielectrics one. Nevertheless, the disambiguation method developed by Miyazaki et al.[9] for the angle θ_r can be applied. In this case, two degree of polarization images have to be acquired with a light rotation of the object.

2.B. Surface Reconstruction

Once the angles θ_r and ϕ are determined, the normals are computed according to the equation (1). To reconstruct the surface shape from the normals, we use the Frankot-Chellappa[17] algorithm. By denoting $\tilde{f}$, $\tilde{p}$, and $\tilde{q}$, the Fourier transforms of respectively the surface height, and the x, y gradients, we have:

$$\forall(u,v) \neq (0,0),\ \ \tilde{f}(u,v) = \frac{-ju\tilde{p} - jv\tilde{q}}{u^2 + v^2}. \tag{11}$$

The surface shape is reconstructed by taking the inverse transform of the former equation. As we can see, this algorithm is only available for surfaces with a null mean slant. Since the derivative, and the Fourier transform are linear operator, the surface can be split according to:

$$f(x,y) = f_0(x,y) + g(x,y), \tag{12}$$

where f_0 is the surface reconstructed from the equation (11) and g is the surface mean plane. g can be deduced by:

$$g(x,y) = x\tilde{p}(0,0) + y\tilde{q}(0,0) + cst, \tag{13}$$

where cst is a constant (integration constant).

This algorithm based on Fourier Transform is less time consuming than the standard algorithm based on relaxation.[18] The shape for 1024×1024 sized images are built in less than one second.

3. Active lighting system

The previous section has shown the ambiguity about the determination of the azimuth angle ϕ from the angle of polarization φ. Miyazaki et al.[9] numerically solve this ambiguity by propagating the information at the occluding boundary to the rest of the object. It implies to get the whole object image, and to assume that the object is geometrically closed, and that all local parts of the surface are not concave toward the camera direction. To solve this ambiguity we propose a new active lighting system.

3.A. Description

Our lighting system is a diffuse dome light (an exploded view is presented on Fig. 4) composed by a ring with numerous LEDs and a dome of which the surface is diffuse. It provides a uniform and unpolarized light onto the object to be digitalized. The ring of LEDs is split into four parts that can be independently electrically controlled. The offset orientation of the dome β belongs to the interval $[0, \pi/2]$.

3.B. Principle

The relation (6) between the angle of polarization φ and the azimuth angle ϕ can be expressed as:

$$\phi = \varphi - \pi/2 + \begin{cases} 0 \\ \pi \end{cases}. \tag{14}$$

To demonstrate the ambiguity solving, a hemisphere was used because it enables to clearly represent all the possible surface orientations. Since the azimuth angle ϕ isn't linked to the refractive index, the azimuth angle image of the hemisphere can be computed nearly all over the surface. Fig. 5(a) and Fig. 5(b) show the azimuth angle images of the hemisphere,

respectively from our acquisition system (without disambiguation), and from the theoretical model. As one can see, π has to be added to the azimuth angle of the points of which the normals are oriented to the north. The splitting of the LEDs ring into two parts would have been sufficient to discriminate the north and south orientations, but it requires a perfect orientation of the dome light: $\beta = 0$.

To disambiguate the azimuth angle ϕ, we firstly compute a segmented image I_{quad} that discriminates the surface points of which the normals are oriented according to the NW, NE, SW or SE directions. Fig. 6 describes the acquisition principle of the segmented image I_{quad} for the hemispheric object. The binary image I_{bin1}, that discriminates the east and west orientations, is obtained by comparing the intensity images acquired with the east and west lighting. In the same way, the binary image I_{bin2} is obtained by comparing the intensity images acquired with the south and north lighting. The segmented image I_{quad}, that discriminates the four orientations, is computed according to the relation: $I_{quad} = 2I_{bin1} + I_{bin2}$. Secondly, π has to be added to the azimuth angle ϕ of which the normals are oriented according to the north direction. Thus, from the azimuth image ϕ (Fig. 5(a)) and from the segmented image I_{quad}, π has to be added to the points of which:

- $I_{quad} = 0$ and $\phi \leq 0$,
- $I_{quad} = 1$,
- $I_{quad} = 3$ and $\phi \geq 0$.

Finally, the algorithm of the disambiguation process can be described according to:

1. $\phi = \varphi - \pi/2$,
2. compute I_{quad},
3. if $[(I_{quad} = 0) \wedge (\phi \leq 0)] \vee [I_{quad} = 1] \vee [(I_{quad} = 3) \wedge (\phi \geq 0)]$, then $\phi = \phi + \pi$,

where $\wedge$ and $\vee$ represent respectively the logical operators AND, OR. The result of the disambiguation is presented Fig.5(c).

4. Experiments

4.A. Experimental set up

The acquisition system is made of a CCD camera, a liquid crystal polarization rotator, and an active diffuse dome light (Fig. 7). The active diffuse dome light is used both to provide an unpolarized light on the whole surface and to solve the ambiguity concerning the azimuth angle. Since the target object is highly specular, it is placed in the center of the dome to be illuminated on most part of its surface. After reflection the light which becomes partially

linearly polarized is studied with the liquid crystal polarization rotator and the camera. The liquid crystal polarization rotator acts like a rotating polarizer, which can electrically be controlled. This device uses nematic liquid crystal cells associated with a linear polarizer, and a quarter wave plate, which provides tunable polarization by changing the supplied voltage. Since the degree of polarization is lower for metallic surfaces, we use a sensitive camera with 10 bits depth. A limitation of the system is due to the hole for the camera, leading to a θ_{min} value which is about 2°. Therefore, the object has to be correctly oriented in order to respect the constraints about the angle θ_r. Nevertheless, approximating the angle θ_r inferior than 2° to $\theta_r = 0°$ (optical axis orientation) doesn't lead to a significant error on the 3D surface reconstruction.

4.B. Quantitative comparisons

The three-dimensional reconstruction of surfaces are both linked to the acquisition system accuracy and to the object shape. Thus, instead of comparing the shape reconstructed from different devices, we have compared the normals. In order to compare the accuracy of the normals acquisition, calibrated hemispheres were used. The norm of the error defined by the following relation was used:

$$\|\vec{e}\| = \|\vec{n}_{th} - \vec{n}_m\|\,, \tag{15}$$

where the subscripts $_{th}$ and $_m$ indicate respectively the theoretical and measured data.

Fig. 8 shows error images taken from three different systems: our polarimetric system, the Replica©500 scanner, and the Minolta©VI-910 scanner. A perfectly specular metallic hemisphere, with a refractive index equal to $\hat{n} = 1.94 + 5.28i$, was used with our system whereas a mat hemisphere was used with the two scanners based on triangulation. The norm of the error is computed with angle θ_r in the interval $[0, 80°]$, meaning that not all the hemisphere surface normals are computed for the three systems in Fig. 8. The error from the polarimetric system is quite random and homogeneous on the surface except on the center, where the normals are oriented near the optical axis. It is both due to the hole in the dome and to the degree of polarization that becomes very small in this region. Indeed, in this case the reflection coefficients are nearly the same, increasing slightly an uncertainty concerning the angle ϕ. Table 1 presents the normals mean error with $\theta_r \in [0, 80°]$ for two different size hemispheres and shows the good accuracy of our system to compute the surface normals.

4.C. Qualitative comparisons

In order to qualitatively compare a 3D surface obtained with our system to a 3D surface of reference, the object was scanned with the Replica 500 scanner. This scanner based on laser ranging, takes regular points with step of 50 μm in X and Y axis, and the precision in Z axis is about 20 μm. The material of the object to study is stainless steel. To compute the

angle θ from the degree of polarization, two issues are possible. The first one, presented in section 2, is to determine directly the angle θ by knowing the refractive index of the object material. The second one is to estimate a pseudo-refractive index, that enables to best fit the relation between the angle θ and the degree of polarization mesured on a known shape of the same material. To determine this index, a known shape of the same material is placed in the center of the dome, and the degree of polarization is measured. Then, a calibration curve, that represents the measured average degree of polarization according to the zenith angle, can be created (Fig. 9). Finally, the Levenberg-Marquardt non-linear algorithm is used to estimate a pseudo-refractive index that best fit the data. This pseudo-refractive index, which has no physical meaning, enables to compute the zenith angle image of the new object by using the relation (10).

Since the Replica scanner is sensitive to the reflectivity of surface, a thin opaque coating has to be applied onto the object. Consequently the details of the object appear clearly more marked with our method rather than with the scanner (Fig. 10(a) and Fig. 10(b)). After registering the 2 surfaces, the mean deviation between the surfaces is about $30\mu m$, meaning that the shape is qualitatively well reconstructed. Moreover, the cross section presented Fig. 11, highlights the good accuracy of the surface computed with our method. The resolutions along the axis X and Y depend only on the used lenses and on the spatial resolution of the sensor: for instance, we are able to get X, Y resolutions 3 times finer compared to the Minolta© scanner.

4.D. Application to 3D inspection

The three-dimensional inspection of highly reflective metallic surfaces is still a delicate task in industrial vision. The aim of our system is to reveal the shape defects on decorations from metallic objects made by stamping and polishing (Fig. 12(a)). Previous work carried out by Seulin[19] was efficient to discriminate geometric aspect defects thanks to a dynamic lighting: by projecting a fringes pattern, defects on smooth surface were revealed near the transition between dark fringes and bright fringes. Nevertheless, this system isn't adapted to inspect shape defects on the objects decorations. With our polarimetric system, the three-dimensional surface of a reference object is computed (Fig. 12(b)). The three-dimensional surface of the objects to be inspected are computed and compared to the reference one. For instance, Fig. 13 shows the photograph and the reconstructed surface of an object with a shape defect on the left-bottom 'bump'. After registering the two shells, the mean deviation between the surfaces is computed (Fig. 14). By this way, our system efficiently discriminates shape defects. The ambiguity problem that appears on the bumps (because normals orientations change from the south to the north) were previously manually solved.[12,13,14] Results shown here present automatic 3D surfaces reconstruction, thanks to the active lighting

system.

5. Conclusions

In this paper, a new way of reconstructing the 3D surface of specular metallic objects is presented. The 'Shape from Polarization' method has been extended to specular metallic surfaces. By using a complex refractive index, and thanks to an approximation commonly used in optics, we have found new relations to compute the normals. Moreover, the active lighting system we developed enables to solve an ambiguity concerning the normals orientation. This new way of disambiguating the azimuth angle is more robust than the numerical methods. Finally, the involved process is quite simple, requiring an active diffuse dome light, a CCD camera and a polarization rotator. The different parts are all electrically controlled, and the three-dimensional surfaces are automatically computed in less than 5 seconds with the presented configuration: 18 polarization images (1024×1024). This acquisition time can drastically be reduced by using faster liquid crystal polarization rotators. The efficiency of the polarimetric system to compute the 3D shape is also presented. An application for inspecting shape defects on metallic specular objects is described. The comparison between a reference surface and a three-dimensional surface to be inspected reveals shape defects. The registration between the two surfaces, required before the comparison, is not automatic yet. Therefore, future works will consist in including an automatic registration in the system.[20,21]

References

1. I. Yun, E. Jung, and S. Lee, "On The Fast Shape Recovery Technique Using Multiple Ring Lights," Pattern Recognition **30**(6), 883–893 (1997).
2. S. Nayar, A. Sanderson, L. Weiss, and D. Simon, "Specular surface inspection using structured highlight and Gaussian images," IEEE Trans. Robotics and Automation **6**(2), 208–218 (1990).
3. S. Savarese and P. Perona, "Local Analysis for 3D Reconstruction of Specular Surfaces," in *IEEE Computer Vision and Pattern Recognition*, vol. 2, pp. 738–745 (Hawaii, USA, 2001).
4. S. Savarese and P. Perona, "Local Analysis for 3D Reconstruction of Specular Surfaces: part II," in *European Conference on Computer Vision*, pp. 759–774 (Copenhagen, Denmark, 2002).
5. J. Zheng and A. Murata, "Acquiring a Complete 3D Model from Specular Motion under the Illumination of Circular-Shaped Light Sources," IEEE Trans. Pattern Analysis and Machine Intelligence **22**(8), 913–920 (2000).
6. K. Koshikawa and Y. Shirai, "A model-based recognition of glossy objects using their polarimetrical properties," Advanced Robotics **2**(2), 137–147 (1987).

7. L. B. Wolff and T. E. Boult, "Constraining Object Features Using a Polarization Reflectance Model," IEEE Trans. Pattern Analysis and Machine Intelligence **13**(7), 635–657 (1991).
8. D. Miyazaki, M. Kagesawa, and K. Ikeuchi, "Determining Shapes of Transparent Objects from Two Polarization Images," in *IAPR Workshop on Machine Vision Applications*, pp. 26–31 (Nara, Japan, 2002).
9. D. Miyazaki, M. Kagesawa, and K. Ikeuchi, "Transparent Surface Modeling from a Pair of Polarization Images," IEEE Trans. Pattern Analysis and Machine Intelligence **26**(1), 73–82 (2004).
10. S. Rahmann, "Inferring 3D Scene Structure from a Single Polarization Image," in *Conference on Polarization and Color Techniques in Industrial Inspection, volume 3826 of SPIE Proceedings, Munich, Germany*, pp. 22–33 (1999).
11. S. Rahmann and N. Canterakis, "Reconstruction of Specular Surfaces Using Polarization Imaging," in *IEEE Computer Vision and Pattern Recognition*, vol. 1, pp. 149–155 (Kauai, USA, 2001).
12. O. Morel, C. Stolz, and P. Gorria, "Application of polarimetric imaging to 3D inspection of highly reflective metallic surface," in *Two- and Three-Dimensional Vision Systems for Inspection, Control, and Metrology II; Kevin G. Harding; ed.*, Proc. SPIE **5606**, 82–89 (2004).
13. O. Morel, C. Stolz, F. Meriaudeau, and P. Gorria, "Polarization imaging applied to 3D inspection of specular metallic surfaces," in *Machine Vision Applications in Industrial Inspection XIII; Jeffery R. Price, Fabrice Meriaudeau; eds.*, Proc. SPIE **5679**, 178–186 (San Jose, California, USA, 2005).
14. O. Morel, C. Stolz, F. Meriaudeau, and P. Gorria, "Three-dimensional inspection of highly-reflective metallic objects by polarization imaging," Electronic Imaging Newsletter **15**(2), 4 (2005).
15. L. B. Wolff, "Polarization Vision: a New Sensory Approach to Image Understanding," Image and Vision Computing **15**(2), 81–93 (1997).
16. M. Born and E. Wolf, *Principles Of Optics*, 7th ed. (Cambridge, 1999).
17. R. Frankot and R. Chellappa, "A Method for Enforcing Integrability in Shape from Shading Algorithms," IEEE Trans. Pattern Analysis and Machine Intelligence **10**(4), 439–451 (1988).
18. K. Ikeuchi, "Determining surface orientations of specular surfaces by using the photometric stereo method," IEEE Trans. Pattern Analysis and Machine Intelligence **3**(6), 661–669 (1981).
19. R. Seulin, F. Merienne, and P. Gorria, "Simulation of specular surface imaging based on computer graphics : application on a vision inspection system," EURASIP Journal on

Applied Signal Processing **2002**(7), 649–658 (2002).

20. P. Besl and N. McKay, "A method for registration of 3-d shapes," IEEE Trans. Pattern Analysis and Machine Intelligence **14**(2), 239–256 (1992).
21. C. Matabosch, J. Salvi, D. Fofi, and F. Meriaudeau, "Range image registration for industrial inspection," in *Machine Vision Applications in Industrial Inspection XIII; Jeffery R. Price, Fabrice Meriaudeau; eds.*, Proc. SPIE **5679**, 216–227 (San Jose, California, USA, 2005).

Table 1. Mean error on normals acquisition

hemisphere diameter	Polarimetric system	Replica Scanner	Minolta scanner
41.275 mm	0.0695	0.0882	0.1034
44.450 mm	0.0644	0.0614	0.0790

List of Figure Captions

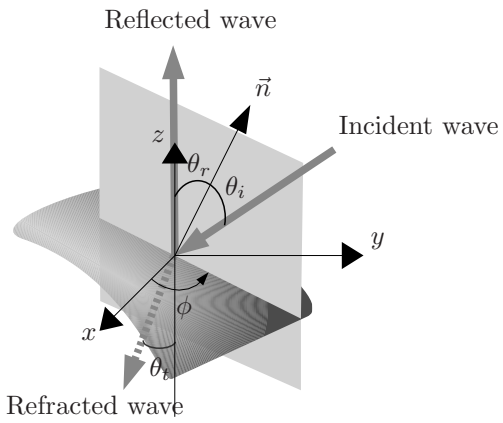

Fig. 1. Light wave reflection on a specular surface. morelF01.eps.

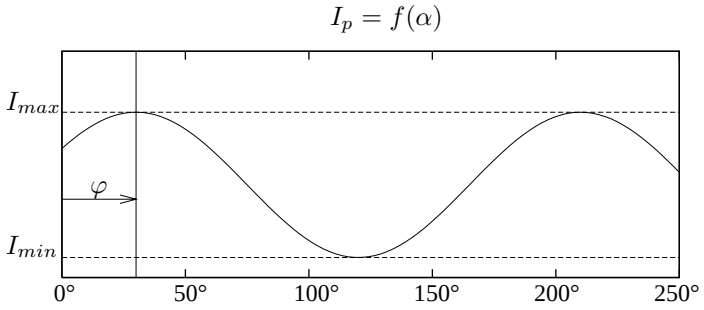

Fig. 2. Variation of the light intensity according to the angle of the polarizer α. morelF02.eps.

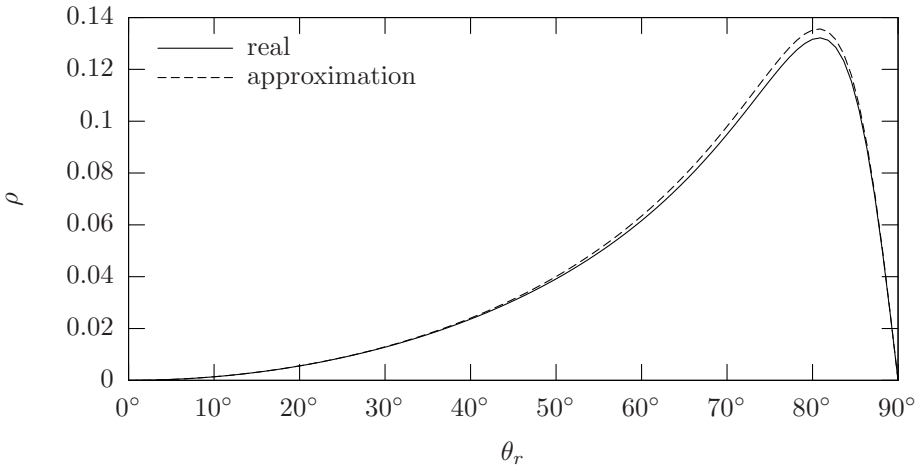

Fig. 3. Comparison between the approximated degree of polarization and the real degree of polarization for a metallic surface ($\hat{n} = 1.94 + 5.28i$). morelF03.eps.

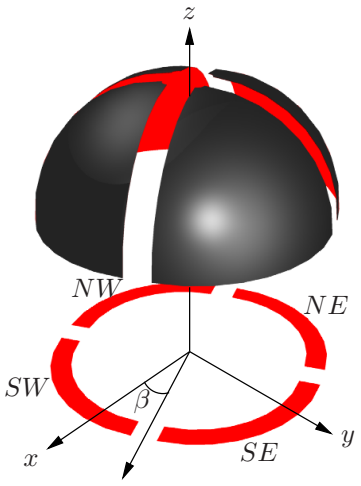

Fig. 4. Exploded view of the active lighting system. morelF04.eps.

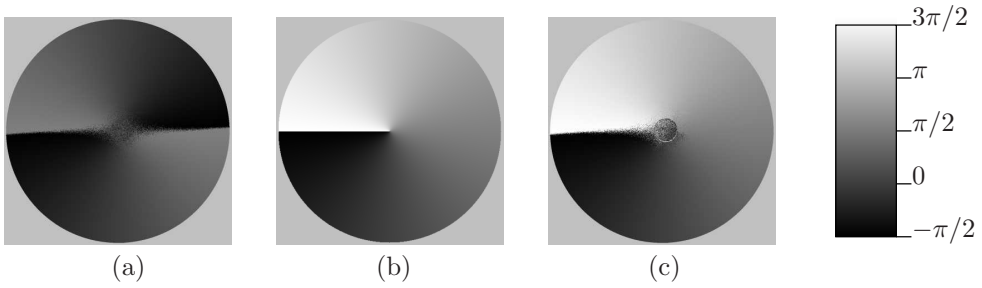

Fig. 5. Disambiguation of the azimuth angle: (a) without disambiguation (ϕ is defined modulo π), (b) theoretical values (ϕ is defined modulo 2π), (c) result of the disambiguation (ϕ is defined modulo 2π). morelF05.eps.

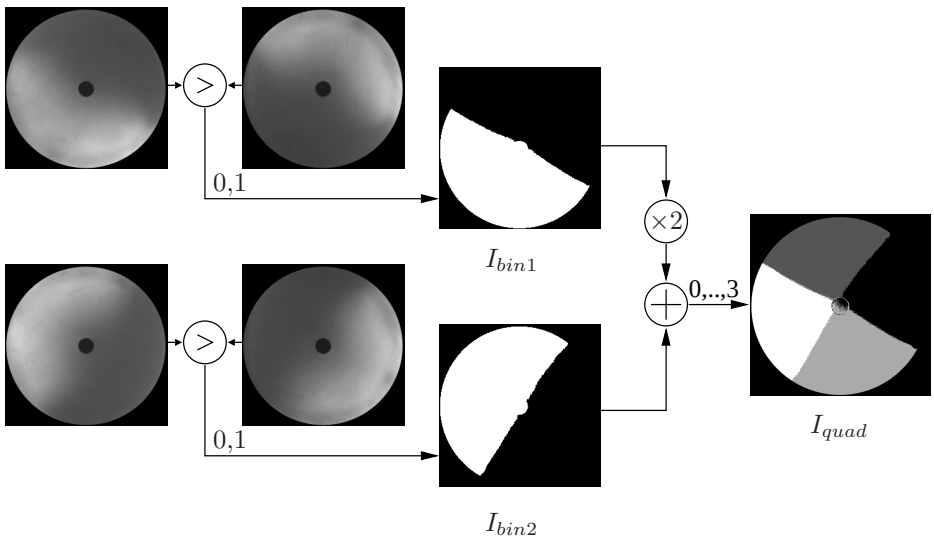

Fig. 6. Acquisition principle of the segmented image I_{quad}. morelF06.eps.

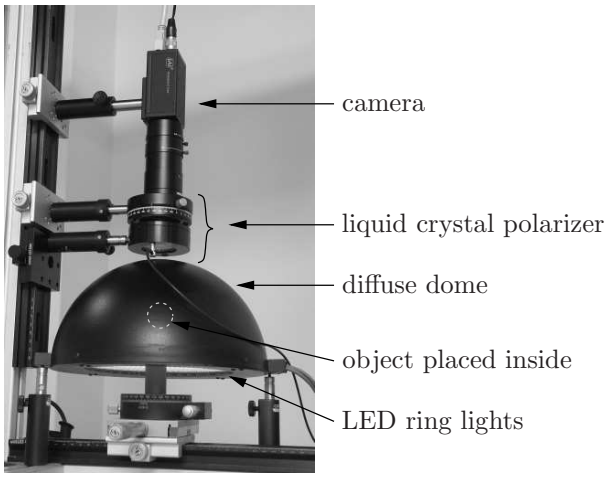

Fig. 7. Experimental set up. morelF07.eps.

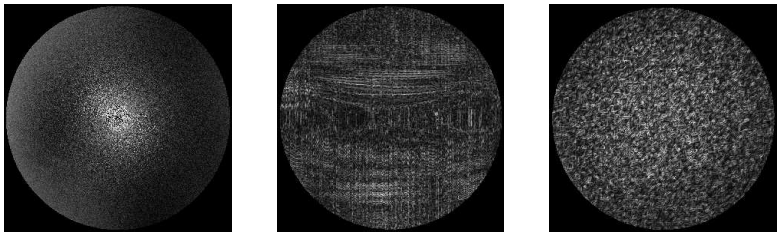

(a) (b) (c)

Fig. 8. Error images of the normals $\|\vec{e}\|$: (a) polarimetric system, (b) Replica scanner, (c) Minolta VI-910 scanner. morelF08.eps.

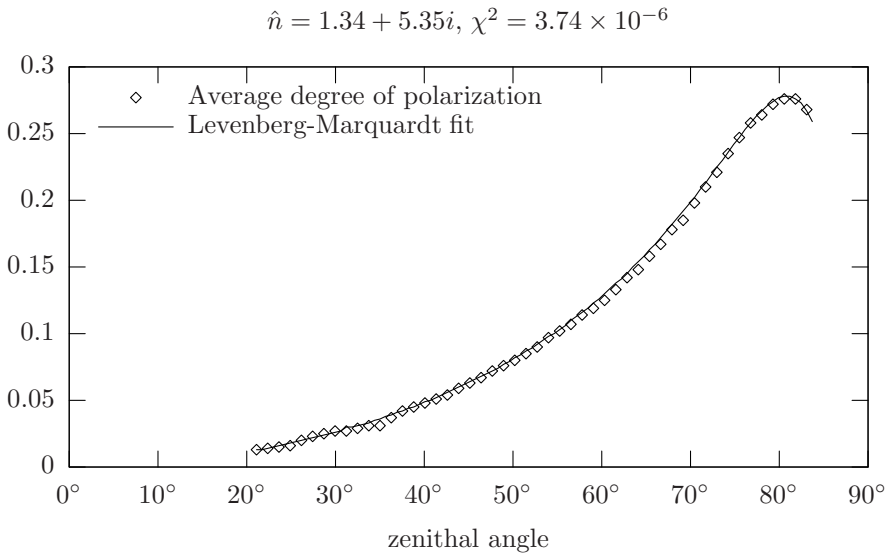

Fig. 9. Calibration curve. morelF09.eps.

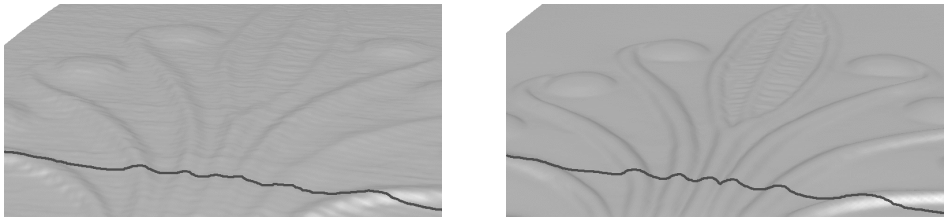

(a) (b)

Fig. 10. 3D reconstruction of a specular metallic object: (a) surface from the 3D scanner, (b) surface from our method. morelF10.eps.

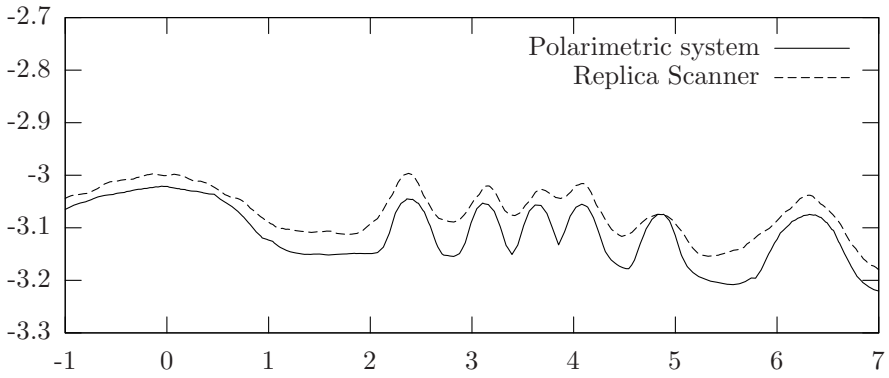

Fig. 11. Comparison of the cross sections (scales given in mm). morelF11.eps.

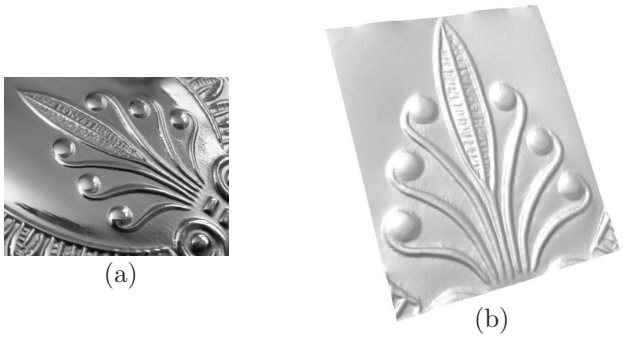

Fig. 12. Object reference photograph (a), and its 3D reconstructed surface (b). morelF12.eps.

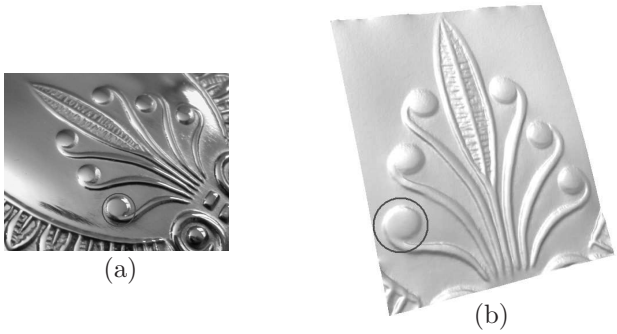

Fig. 13. Object with a shape defect photograph (a), and its 3D reconstructed surface (b). morelF13.eps.

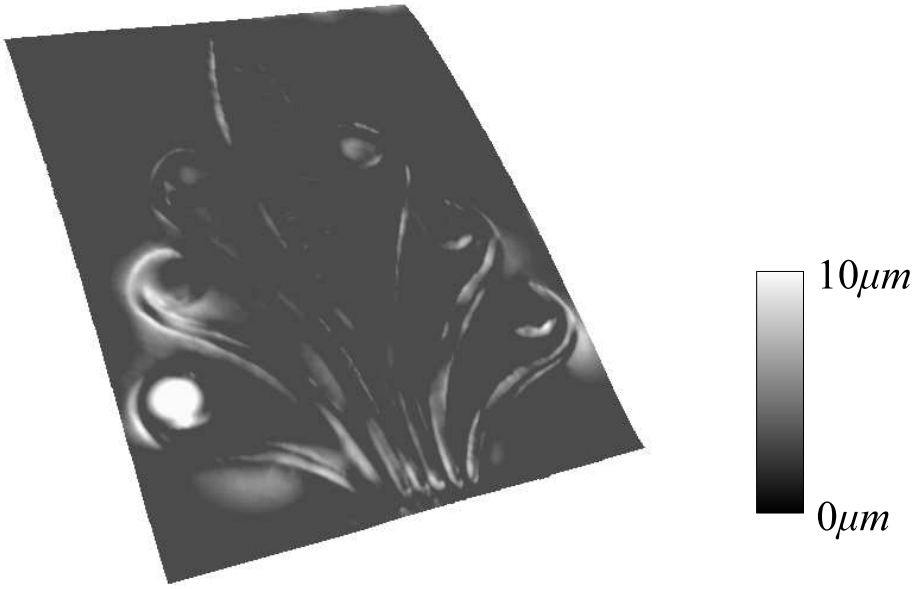

Fig. 14. Mean deviation between the two reconstructed surfaces. morelF14.eps.